4

Measurement of Brain Function Using Near-Infrared Spectroscopy (NIRS)

Hitoshi Tsunashima, Kazuki Yanagisawa and Masako Iwadate
Nihon University
Japan

1. Introduction

Near-infrared spectroscopy (NIRS) has gained attention in recent years (Hoshi et al., 2001; Tamura, 2003). This non-invasive technique uses near-infrared light to evaluate increases or decreases in oxygenated hemoglobin or deoxygenated hemoglobin in tissues below the body surface.

NIRS can detect the hemodynamics of the brain in real time while the subject is moving. Brain activity can therefore be measured in various environments. Recent research has used NIRS to measure brain activity in a train driver (Kojima et al., 2005, 2006). NIRS has also been used to evaluate the mental activity of an individual driving a car in a driving simulator (Shimizu et al., 2009).

Various arguments have focused on interpretation of signals obtained from NIRS, and no uniform signal-processing method has yet been established. Averaging and baseline correction are conventional signal-processing methods used for the NIRS signal. These methods require block design, an experimental technique that involves repeating the same stimuli (tasks) and resting multiple times in order to detect brain activation during a task. However, brain activation has been noted to gradually decline when a subject repeats the same task multiple times (Takahashi et al., 2006).

Fourier analysis, which is frequently used for signal analysis, transforms information in the time domain into the frequency domain through the Fourier transform. However, time information is lost in the course of the transform. As the NIRS signal fluctuates, time-frequency analysis is suitable for the NIRS signal.

The wavelet transform is an efficient method for time-frequency analysis (Mallat, 1998). This approach adapts the window width in time and frequency so that the window width in frequency becomes smaller when the window width in time is large, or the window width in frequency becomes larger when the window width in time is small. Multi-resolution analysis (MRA) (Mallat, 1989) decomposes the signal into different scales of resolution. MRA with an orthonormal wavelet base effectively facilitates complete decomposition and reconstruction of the signal without losing original information from the signal.

Oxygenated hemoglobin and deoxygenated hemoglobin as measured in NIRS are relative values from the beginning of measurement and vary between subjects and parts of the brain. Simple averaging of the NIRS signal thus should not be applied for statistical analysis. To solve this problem, we propose the Z-scored NIRS signal.

The aim of this chapter is to propose a signal processing method suitable for the NIRS signal and applicable for neuroimaging studies. We first describe the principle underlying measurement of brain activity with NIRS in Section 2. We then propose discrete wavelet-based MRA to extract the task-related signal from original NIRS recordings in Section 3.
In Section 4, we describe simultaneous measurement experiments with NIRS and functional magnetic resonance imaging (fMRI) using mental calculation tasks to confirm the validity of the proposed signal processing method. To investigate relationships between brain blood flow and skin blood flow, measurement is carried out using NIRS and the laser Doppler skin blood flow probe. The Z-scored NIRS signal is proposed for statistical analysis.
Two application examples with the proposed method for NIRS signals are shown in Section 5. We demonstrate the possibility of using the proposed method for evaluating brain activity associated with driving a car in a realistic driving environment. Another application is to brain-computer interfaces (BCIs), which are used in actively conducted studies. A BCI is a system that controls machines and devices by extracting neural information from human brain activity. BCIs are expected to become prominent as nursing robotics, such as artificial hands. The proposed method is applied for BCI systems that can control a robot arm using NIRS. We measured brain activity during actual grasping tasks and imagined grasping tasks using the BCI system to demonstrate the validity of the proposed BCI system.
Finally, some conclusions are given in Section 6.

2. Near-infrared Spectroscopy (NIRS)

Using near-infrared rays, NIRS non-invasively measures changes in cerebral blood flow. The principle of measurement was developed by Jöbsis (1977), based on the measurement of hemoglobin oxygenation in the cerebral blood flow.
In uniformly distributed tissue, incident light is attenuated by absorption and scattering. The following expression, a modified Lambert-Beer law, was therefore used:

$$Abs = -\log(I_{out} / I_{in}) = \varepsilon \bar{l} C + S \,. \tag{1}$$

Here, I_{in} is the irradiated quantity of light; I_{out} is the detected quantity of light; ε is the absorption coefficient; C is the concentration; $\bar{l}$ is the averaged path length; and S is the scattering term.
If it is assumed that no scattering changes in brain tissue occur during activation of the brain, the change in absorption across the activation can be expressed by the following expression:

$$\Delta Abs = -\log(\Delta I_{out} / \Delta I_{in}) = \varepsilon \bar{l} \Delta C(\Delta X_{oxy}, \Delta X_{deoxy}) \,. \tag{2}$$

Furthermore, if the change in concentration (ΔC) is assumed to be proportional to the changes in oxygenated hemoglobin (ΔX_{oxy}) and deoxygenated hemoglobin (ΔX_{deoxy}), the following relational expression can be obtained:

$$\Delta Abs(\lambda_i) = \bar{l}[\varepsilon_{oxy}(\lambda_i)\Delta X_{oxy} + \varepsilon_{deoxy}(\lambda_i)\Delta X_{deoxy}] \,. \tag{3}$$

The absorption coefficients of oxygenated hemoglobin and deoxygenated hemoglobin at each wavelength, $\varepsilon_{oxy}(\lambda_i)$ and $\varepsilon_{deoxy}(\lambda_i)$, are known. As a result, $\overline{l}\Delta X_{oxy}$ and $\overline{l}\Delta X_{deoxy}$ can be obtained by performing measurements with near-infrared rays of two different wavelengths and solving Equation 3. However, the quantity obtained here is the product of the change in concentration and the averaged path length. In general, this averaged path length $\overline{l}$ varies greatly from one individual to another, and from one part of the brain to another. Caution must therefore be exercised in evaluating the results.

3. Signal processing methods for NIRS

3.1 Recording of NIRS signal

As mental calculation tasks, a low-level task comprising simple one-digit addition (e.g., 3 + 5) and a high-level task comprising subtraction and division with a decimal fraction (e.g., 234/(0.61 − 0.35)), were set to obtain NIRS signals. Brain activity in the prefrontal lobe was measured using NIRS. The measurement instrument was the OMM-3000 multichannel NIRS system (Shimadzu Corporation, Japan) (Kohno, 2006).

Figure 1 illustrates the arrangement of optical-fiber units and the location of each channel (3×7 matrix, 32 channels). Figure 2 shows the recorded temporal histories of oxygenated hemoglobin (red line, indicated as oxy-Hb) and deoxygenated hemoglobin (blue line, indicated as deoxy-Hb) in channel 20.

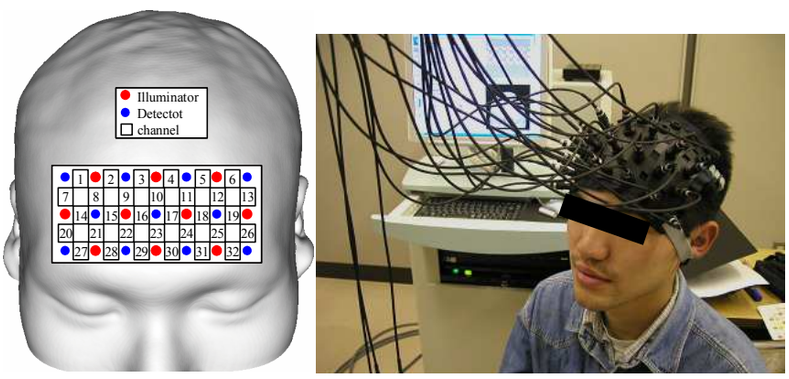

Fig. 1. Position of optical fibers and channels for recording NIRS signals (mental calculation task: matrix, 32 channels)

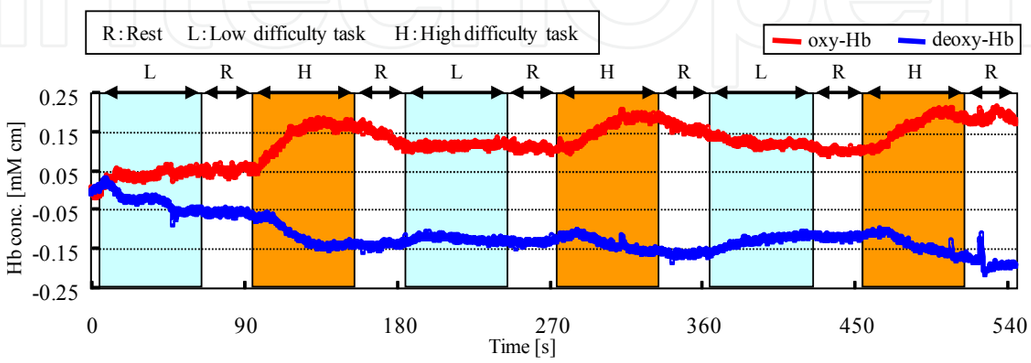

Fig. 2. Temporal history of NIRS signals in mental calculation (channel 20)

3.2 Analysis of NIRS signals

In NIRS signal analysis, brain activity related to a task must be separated from that which is not, since NIRS measures not only signals of brain activity during a task, but also other signals, including measurement noise.

In general, changes in oxygenated hemoglobin and deoxygenated hemoglobin when the brain is activated and restored to the original state exhibit the trend illustrated in Figure 3 (Huettel, 2004). Therefore, if these signals can be extracted from the measured signals, the brain has obviously been activated.

Averaging and baseline correction are conventional signal-processing methods. These methods require block design, an experimental technique that involves repeating the same stimuli (tasks) and resting multiple times in order to detect brain activation during a task.

Averaging is the method by which data are averaged for each task. Randomly generated noise approaches zero with averaging, and only periodic data are left. Averaging is effective when similar reactions are generated repeatedly. However, for cerebral blood flow that shows large variations in reactions to the same stimuli, the reliability of averaged signals is low, and false signals may be created. Furthermore, even significant signals may become undetectable after averaging.

Baseline correction corrects the start and end points of a block to zero to remove gradual trends, based on the assumption that blood flow is restored to its original state during a task block. However, because blood flow involves irregular fluctuations, the reference points are unstable. Therefore, if the whole block is corrected based on those two points alone, signals may be distorted.

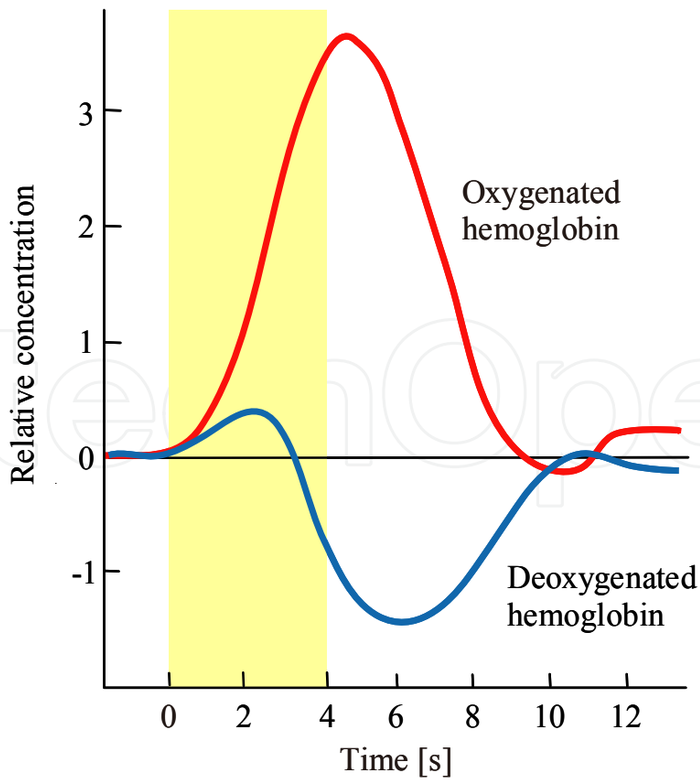

Fig. 3. Schematic of changes in hemoglobin concentration due to neural activity

Figure 4 shows the result of baseline correction applied for NIRS signals (Fig. 2) after removing high-frequency noise using a moving average of 25 data. Figure 5 indicates the functional brain imaging of the frontal lobe. It should be noted that brain activation gradually declines when a subject repeats the same task multiple times.

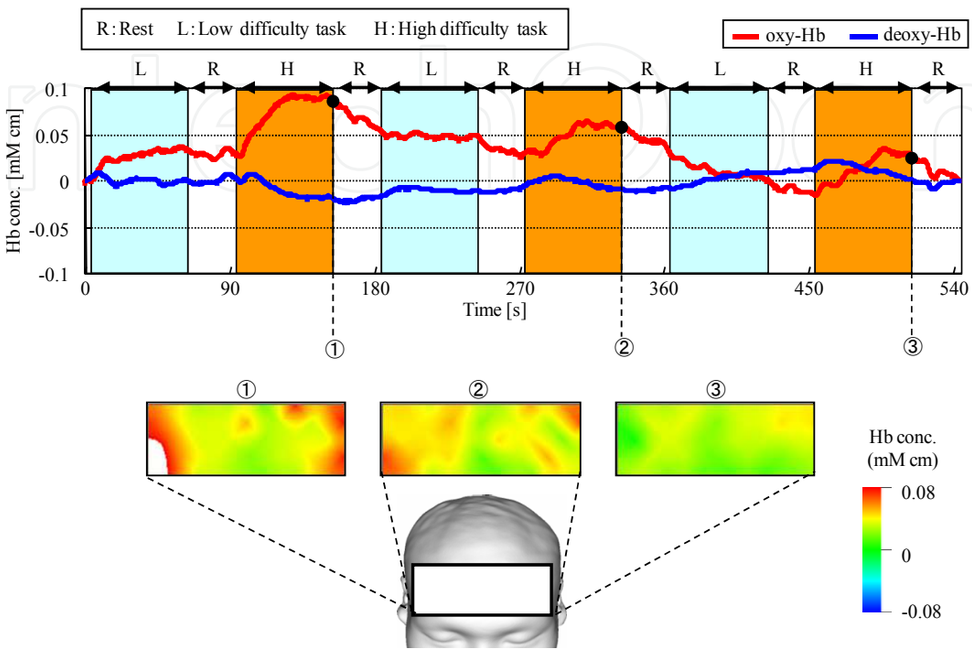

Fig. 4. Results of signal processing with baseline correction and de-noising

3.3 Decomposition and reconstruction of NIRS signals using wavelet transform

3.3.1 Wavelet transform

Fourier analysis, which is frequently used for frequency analysis, transforms information in the time domain into information in the frequency domain through the Fourier transform. However, time information is lost in the course of the transform.

A short-time Fourier transform, or windowed Fourier transform, can be used for time-frequency analysis of signals. However, the detection capacity varies widely, depending on the setting of the window.

In contrast, wavelet transform is an efficient method of time-frequency analysis. This approach adapts the window width in time and frequency so that the window width in frequency becomes smaller when the window width in time is large, or the window width in frequency becomes larger when the window width in time is small.

Wavelet transform expresses the local shape of the waveform to be analyzed, $S(t)$, by shifting and dilating the waveform called the mother wavelet, $\psi(t)$, and then analyzes the waveform.

A wavelet ψ is a function of zero average

$$\int_{-\infty}^{+\infty} \psi(t)dt = 0 \tag{4}$$

which is dilated with a scale parameter a and translated by b as

$$\psi_{a,b}(t) = \frac{1}{\sqrt{a}}\psi(\frac{t-b}{a}) . \quad (5)$$

The continuous wavelet transform of signal $S(t)$ is computed with $\psi_{a,b}(t)$ as

$$\tilde{S}(a,b) = \int_{-\infty}^{\infty} S(t)\psi^*_{a,b}(t)dt . \quad (6)$$

Here, ψ^* denotes the complex conjugate of ψ.
One can construct wavelets ψ such that the dilated and translated function

$$\psi_{m,n}(t) = 2^{-m/2}\psi(2^{-m}t - n) \quad (7)$$

is an orthonormal base. Discrete wavelet transform can be computed by

$$D_m = \int_{-\infty}^{\infty} S(t)\psi_{m,n}(t)dt . \quad (8)$$

In the continuous wavelet transform, information is duplicated, requiring many calculations. Discrete wavelet transform handles a smaller volume of information than continuous wavelet transform, but is able to transform signals more efficiently. Furthermore, use of an orthonormal base facilitates complete reconstruction of original signals without redundancy. The following section describes decomposition and reconstruction of signals using MRA.

3.3.2 Multi-Resolution Analysis (MRA)

MRA decomposes signals into a tree structure using the discrete wavelet transform. In the case of the object time-series signals, $S(t)$, it decomposes the signals into an approximated component (low-frequency component) and multiple detailed components (high-frequency components).
A signal $S(t)$ can be expressed as follows by discrete wavelet transform using an orthonormal base $\psi_{m,n}$ as

$$S(t) = \sum_{n=-\infty}^{\infty} A_{m_0,n}\phi_{m_0,n}(t) + \sum_{m=-\infty}^{m_0}\sum_{n=-\infty}^{\infty} D_{m,n}\psi_{m,n}(t) . \quad (9)$$

Here, $\phi_{m,n}(t)$ is the scaling function as defined by the following equation:

$$\phi_{m,n}(t) = 2^{-m/2}\phi(2^{-m}t - n) . \quad (10)$$

The coefficient of the approximated component is calculated by

$$A_{m,n} = \int_{-\infty}^{\infty} S(t)\phi_{m,n}(t) . \quad (11)$$

The detailed components of the signals on level m can be expressed by

$$d_m = \sum_{n=-\infty}^{\infty} D_{m,n}\psi_{m,n}(t) \,. \tag{12}$$

Thus, signal $S(t)$ can be expressed as

$$S(t) = a_{m_0} + \sum_{m=-\infty}^{m_0} d_m \,. \tag{13}$$

Task-related components can thus be reconstructed from detailed components d_m.

In the wavelet transform, the choice of a mother wavelet $\psi_{m,n}$ is important. We employed a *Daubechies* wavelet (Daubechies, 1992), which is orthonormal base and is a compactly supported wavelet. The vanishing moments of the *Daubechies* wavelet can be changed by an index *N*. We decided to use a relatively high-order generating index, *N* = 7.

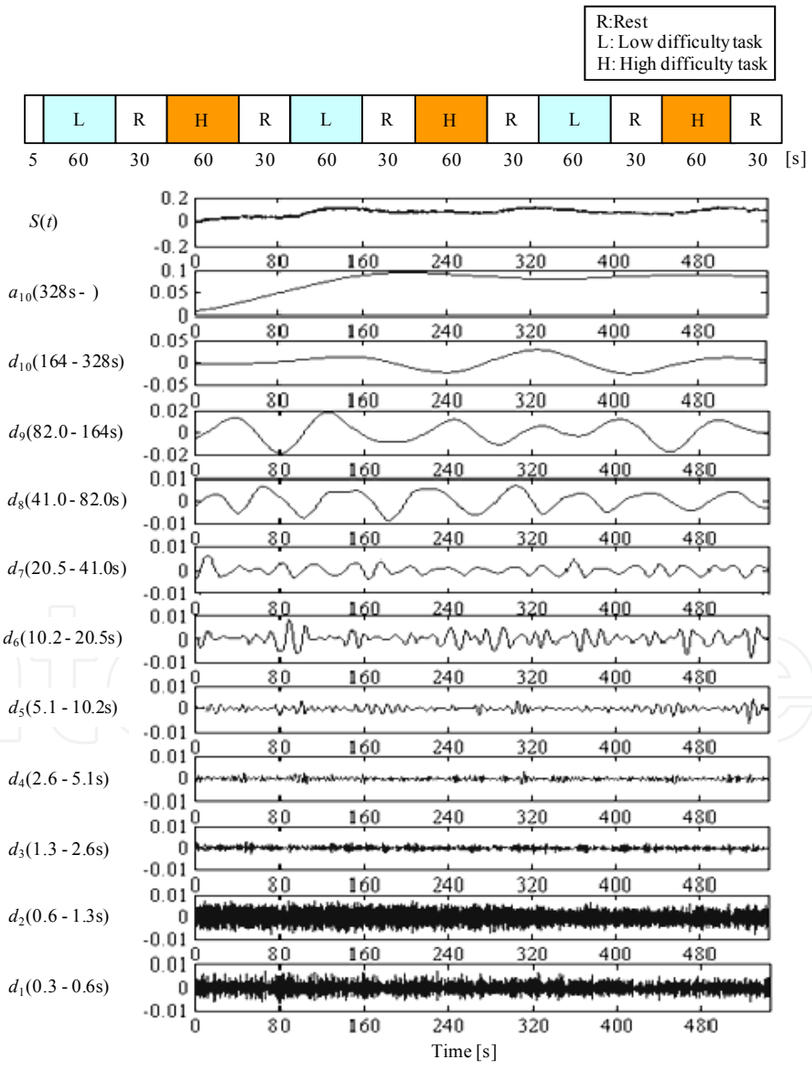

Fig. 5. Decomposition of NIRS signal using a wavelet base (*Daubechie* 7)

Figure 5 presents MRA results for oxygenated hemoglobin in channel 20, where task-related changes were marked. Here, the measured signal was decomposed into ten levels. The trend of the whole experiment was extracted on the approximated component (a_{10}), in the lowest-frequency range.

Here, d_1 and d_2, the highest frequency ranges, showed a relatively large amplitude. It is possible that these ranges represented measurement noise. As the interval for repetition of tasks and rests was 64 s, the d_8 component was the central component of task-related changes. Signals were therefore reconstructed by adding the d_7, d_8, and d_9 components.

Reconstructed signals are illustrated in Figure 6. Of note, the activation pattern of oxygenated hemoglobin and deoxygenated hemoglobin, shown in Figure 3, can be observed very clearly. Comparison between Figure 4 (signal processing with baseline correction and de-noising) and Figure 6 (wavelet-based method) shows the improved performance of the proposed method. Results revealed that oxygenated hemoglobin increased and the brain was activated during mental calculation tasks.

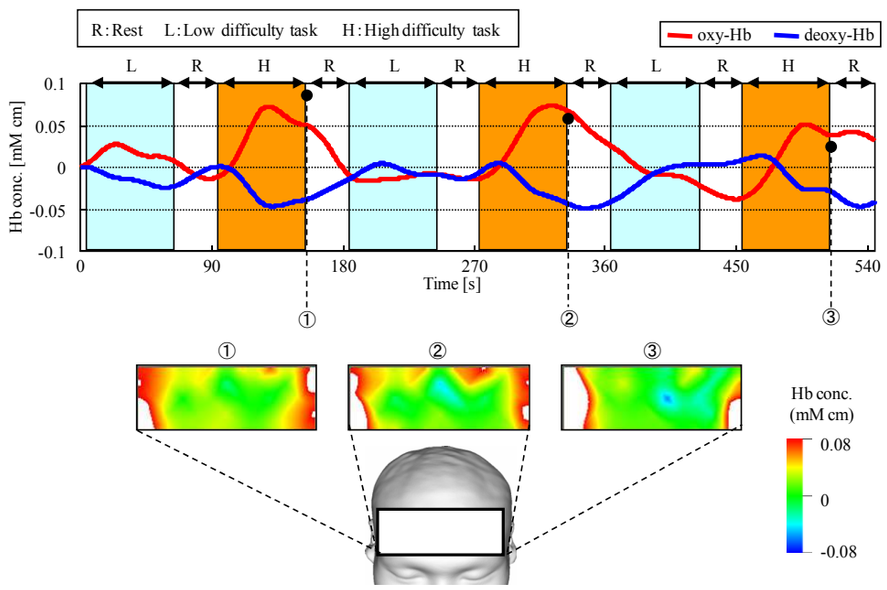

Fig. 6. Results of brain imaging using reconstructed signals

4. Measurement of brain functions under mental workload

4.1 Setting of workload

To confirm the validity of the signal-processing method explained in the previous section, we measured brain functions through simultaneous use of NIRS and fMRI.

To measure brain activity under workload, we used the workload of mental calculation. Mental calculation tasks were set to low, medium, and high levels as follows:

- Low-level task: Simple one-digit addition (e.g., 3 + 5)
- Medium-level task: One-digit addition of three numbers (e.g., 6 + 5 + 9)
- High-level task: Subtraction and division with decimal fraction (e.g., 234/(0.61 − 0.35))

The design of the experiment is presented in Figure 7. Each set was composed of 28 s of task and 36 s of rest, in that order. By arranging three sets for each level in random order, a total of nine sets of experiment were conducted over 592 s.

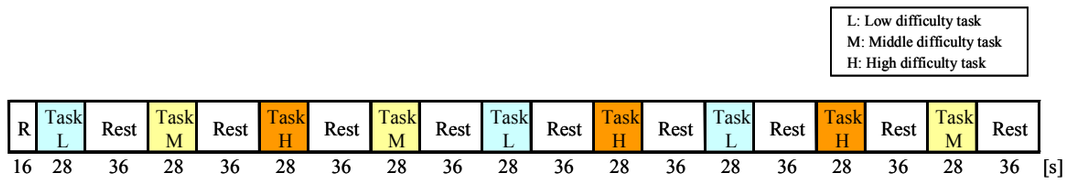

Fig. 7. Experimental design

A 28s task consisted of 14 questions at 2s intervals for the low level, 10 questions at 2.8s intervals for the intermediate level, or two questions at 14s intervals for the high level. The subject answered the questions displayed on the computer monitor without speaking. During the 36s rest time, the subject rested while steadily gazing at a cross mark displayed on the computer monitor.

4.2 NIRS and fMRI signal recording

Brain activity in the prefrontal lobe was measured using NIRS and fMRI simultaneously. NIRS data were collected using the OMM-3000 system (Shimadzu Corporation, Japan) in the MRI scanner.

Data from fMRI (3 mm thickness, 40 slices) were collected using a Siemens Symphony 1.5T (T2*-weighted gradient-echo sequence, TR = 4000 ms, TE = 50 ms, FA = 90 degrees, 64×64 pixels, FOV = 192 mm). Whole-brain images were obtained as T1-weighted images (TR = 2200 ms, TE = 3.93 ms, FA = 15 degrees, TI = 1100 ms, 1 mm^3 voxel, FOV = 256 mm).

Data from fMRI were pre-processed using Statistical Parametric Mapping (SPM99; Welcome Department of Imaging Neuroscience, UK) Normalized contrast images were smoothed with an isotropic Gaussian kernel (FWHM = 12 mm). Regions of interest (ROIs) were defined as clusters of 10 or more voxels in which estimated parameter values differed significantly from zero ($p<0.01$).

Subjects were nine healthy volunteers (nine men, no women). The arrangement of optical fiber units and measurement positions is shown in Figure 1.

4.3 Signal processing

Figure 8 presents measurement results through all channels for Subject A during the first three tasks. During the mental calculation task at the high level (i.e., the third task), oxygenated hemoglobin increased and deoxygenated hemoglobin decreased on both outer sides of the frontal lobe.

Figure 9 presents MRA results for oxygenated hemoglobin in channel 26, where task-related changes were marked. The trend of the whole experiment was extracted on the approximated component (a_{10}). As the interval of repetition of tasks and rests was 64 s, the d_8 component was the central component of task-related changes. Signals were thus reconstructed by adding the d_7, d_8, and d_9 components.

Reconstructed signals from channel 26 are illustrated in Figure 10. Results revealed that oxygenated hemoglobin increased and the brain was activated during mental calculation tasks. Furthermore, such changes became larger as the level of mental calculation task increased.

Figure 11 shows a comparison of functional brain imaging by fMRI and NIRS with the proposed method. The rectangle in the fMRI image indicates the region of measurement with NIRS. NIRS images agree with those for fMRI at a different workload level. This result supports the effectiveness of MRA with the discrete wavelet transform.

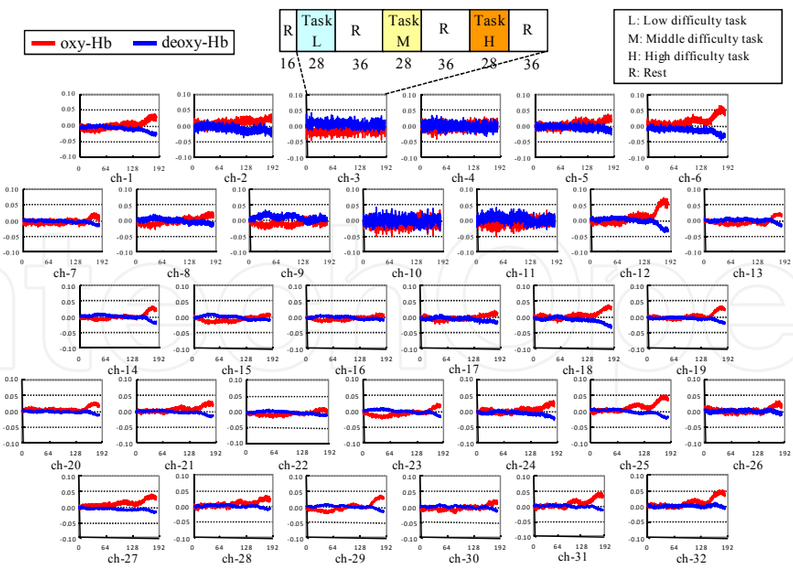

Fig. 8. Hemoglobin concentration changes in frontal lobe

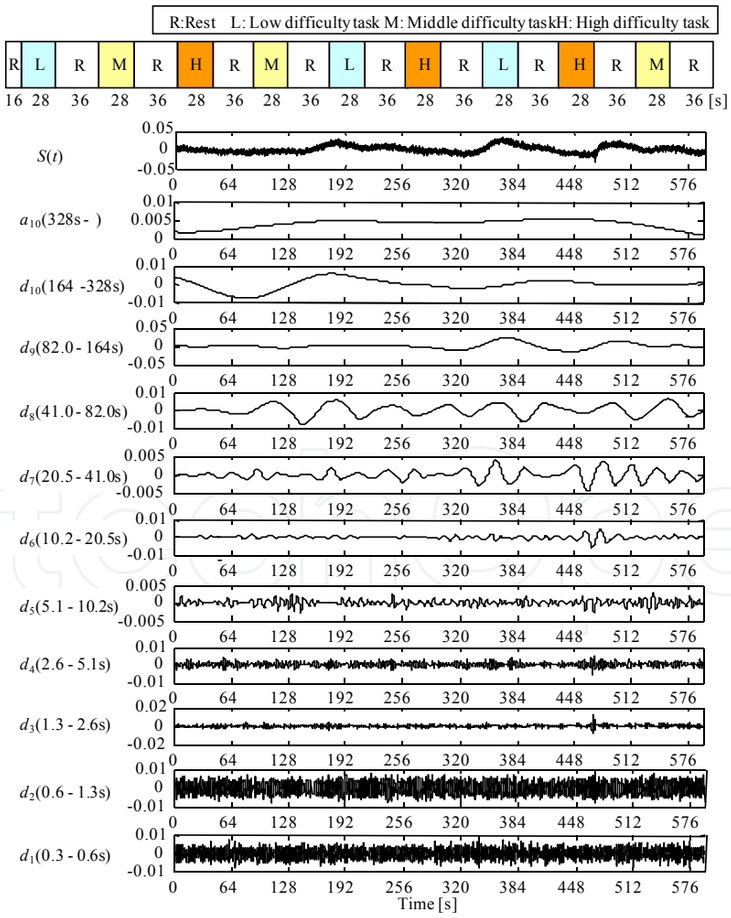

Fig. 9. Decomposition of NIRS signal (channel 26)

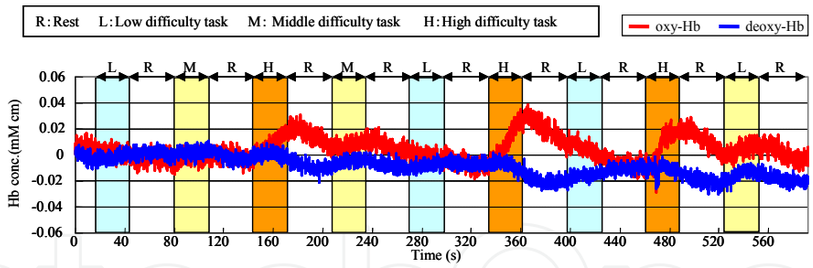

(a) Original signal

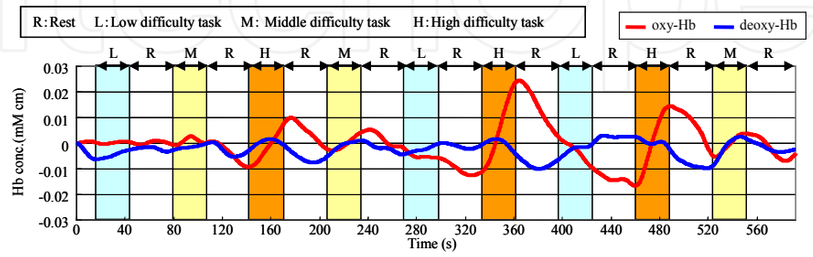

(b) Reconstructed NIRS signal

Fig. 10. Comparison of original signal and reconstructed signal (channel 26)

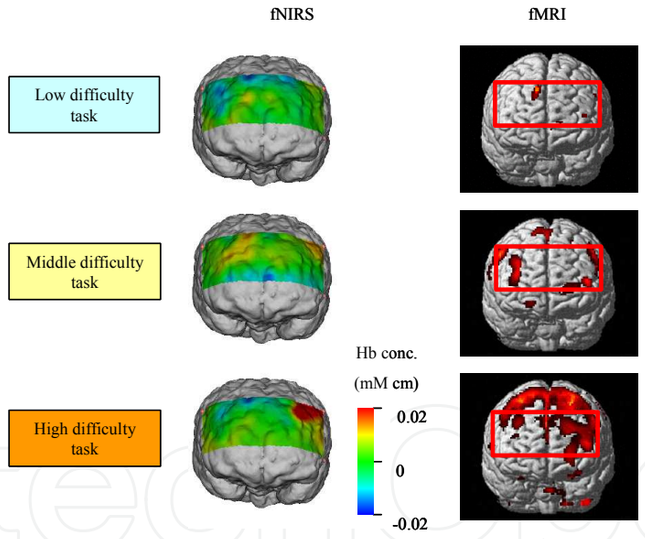

Fig. 11. Functional brain imaging by fMRI and NIRS

4.4 Influence of skin blood flow (SkBF)

To investigate relationships between brain blood flow and SkBF, we took measurements using NIRS and the laser Doppler SkBF probe. The laser Doppler SkBF probe (Advance Corporation, Japan) was placed on the right side of the forehead, 5 cm from the nasal root. The semiconductor laser Doppler velocimeter used a monochromatic light source at 780 nm. Figure 12 shows the comparison of NIRS signal (cerebral blood flow) and SkBF. Oxygenated hemoglobin increased and the brain was activated during mental calculation tasks. Furthermore, such changes became larger as the level of mental calculation task increased. But, SkBF did not increase in relation to task level.

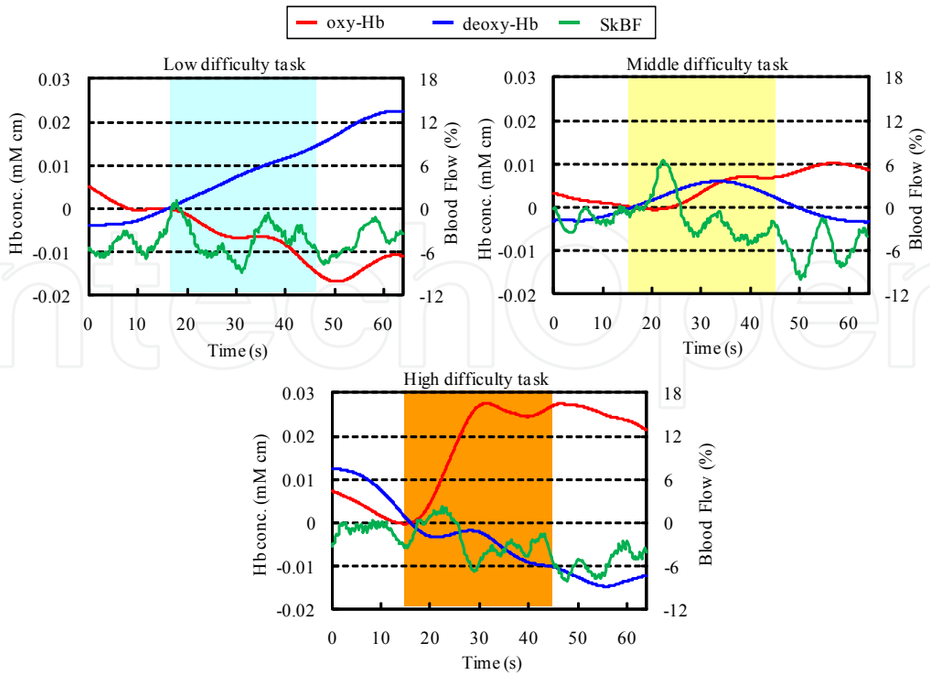

Fig. 12. Comparison of NIRS signal (channel 26) and SkBF

Mean values of oxygenated hemoglobin and SkBF at each task level are shown in Figure 13. The mean value of NIRS (Fig. 13(a)) became higher with higher task level. However, the mean value of SkBF (Fig. 13(b)) did not change in relation to task level. This result confirmed that SkBF did not influence NIRS signals (cerebral blood flow) in the recognition task.

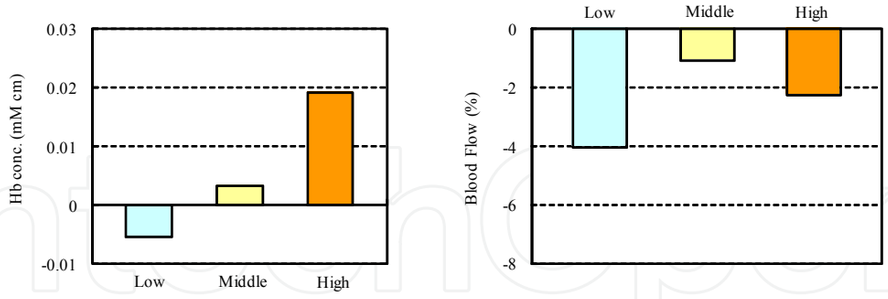

(a) Result of oxy-Hb mean value (b) Result of SkBF mean value

Fig. 13. Averaged result for oxy-Hb and SkBF at each task level

4.5 Statistical analysis

The NIRS signal expresses the quantity of relative changes using the start point as the reference. However, comparisons of measurements between subjects or statistical processing of measurements of all subjects cannot be implemented using this signal as is. Therefore, we propose a method for converting data of oxygenated hemoglobin and deoxygenated hemoglobin reconstructed by MRA into Z-scores using the following expression, so that the mean value is 0 and standard deviation is 1.

$$Z = \frac{X - \mu}{\sigma} \tag{14}$$

Here, X is the signal of oxygenated hemoglobin or deoxygenated hemoglobin reconstructed using MRA; μ is the mean value; and σ is the standard deviation.

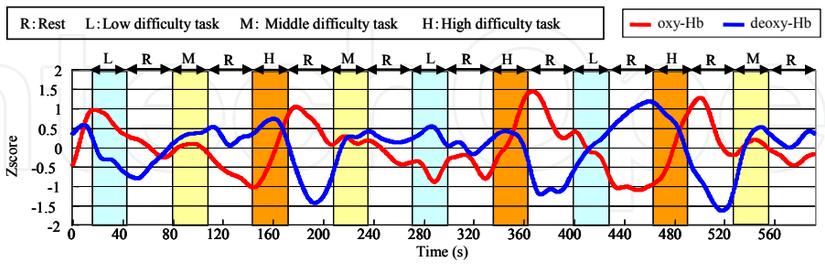

(a) Averaged reconstructed fNIRS signal (channel 26)

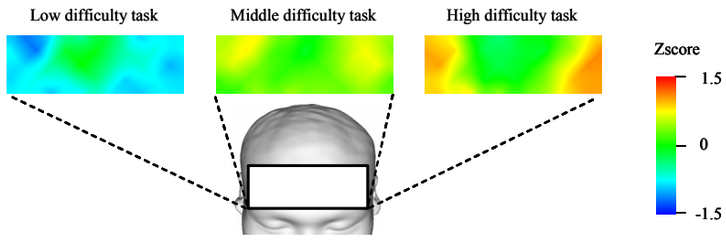

(b) Brain activity imaged by averaged NIRS signals

Fig. 14. Results of group analysis of NIRS signals for nine subjects

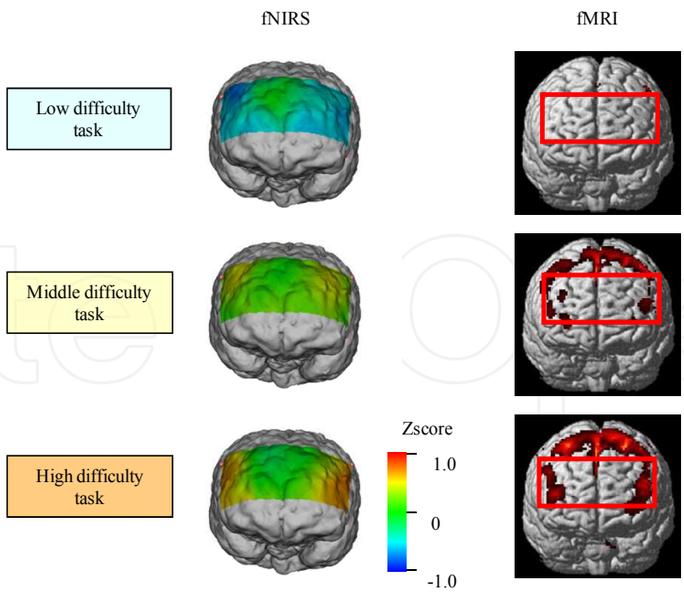

Fig. 15. Functional brain imaging by fMRI and NIRS (group analysis for nine subjects)

Figure 14 shows averaged NIRS signals using Z-score for nine subjects. Of note, the difference in workload level is reflected in the gradient of the oxygenated hemoglobin

concentration. Figure 15 shows the results of group analysis for nine subjects. The rectangle in the fMRI image indicates the region of measurement with NIRS. NIRS images agree with results of fMRI regarding different workload levels. This result supports the effectiveness of the proposed method.

4.6 Subjective and objective evaluation of workload

In this experiment, the workload of each subject was measured using the Japanese version of NASA-TLX to evaluate correlations between the workload of mental calculation tasks and the objective evaluation using NIRS. The NASA-TLX is composed of six measures: mental requirements; physical requirements; temporal demand; work performance; effort; and frustration. Before workload evaluation, the subject performed one-to-one comparisons of the importance of elements of the workload involved in task performance.

The weight of each measure was based on the number of times an element was selected as more important during 15 one-to-one comparisons. When evaluating the workload of each task, the subject placed a mark at the appropriate position on the segment drawn between both extremes for each of the six measures.

A weighted workload (WWL) score was obtained by reading the position of each evaluation mark on a scale of 0 to 100 and multiplying by the weight for each measure determined by one-to-one comparison, then averaging all the products. Figure 16 (left) presents the WWL score of Subject A as determined by NASA-TLX. Workload became higher with higher task level.

Figure 16 (right) shows the results for 9 subjects evaluated using the maximum gradient of oxygenated hemoglobin in the task with different workload levels. Multivariate test using the Ryan method was used. Significant differences between high- and low-level tasks, or between high- and medium-level tasks are apparent ($p<0.05$). The results exhibited good correlation with subjective evaluation using NASA-TLX. This result confirms the feasibility of evaluating workload using the signal of cerebral blood flow obtained from NIRS.

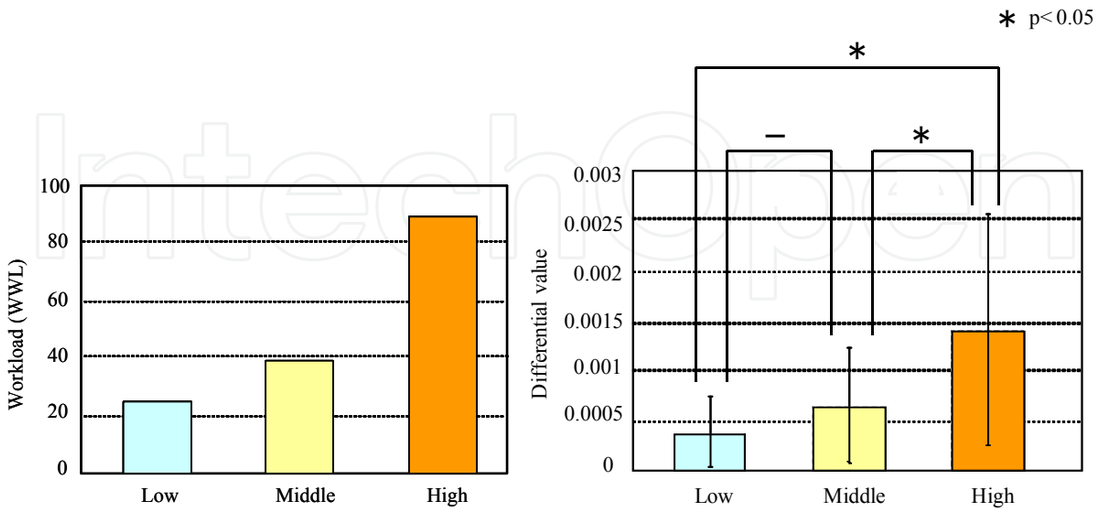

(a) Workload evaluation by NASA-TLX. (b) Maximum gradient of NIRS signal during the task

Fig. 16. Subjective and objective evaluation of workload

5. Application examples

5.1 Measurement of brain functions while driving a car

5.1.1 Background

Car drivers obtain visual information on the surrounding environment, recognize and judge that information suitably and then control their vehicle using the steering wheel, accelerator and brake pedal operations. Human brain activity functions to control all of these processes. In situations where it is necessary to predict unexpected danger, brain activity of the driver is thought to strengthen the cognitive function by spontaneously raising the level of attention. In the course of developing driver support systems, having a clear understanding of human brain activity is important in such driving situations.

In recent years, various driving-assistance systems have been developed to improve safety by reducing driver workloads. Examples include the adaptive cruise control (ACC) system, which maintains a safe distance between the driver's vehicle and the vehicle ahead, and the lane-keeping assistance system, which keeps the car in a lane through steering support.

However, while driver workload is reduced, the attention of the driver may also be reduced, resulting in unexpected accidents. Driver workload thus needs to be examined from the perspectives of cognitive engineering and human physiology. It is necessary to clarify relationships between driver workload and brain activity, which includes recognition and judgment. Driver attention then needs to be evaluated and the relationship between brain activity and driving performance clarified.

A small number of neuroimaging studies have used driving simulators to examine brain activity during driving. In these studies (Uchiyama, 2003; Spiers & Maguire, 2007), fMRI has been used. However, fMRI has many shortcomings in evaluating driving performance, requiring the subject to lie in a narrow cylinder during evaluation and not permitting movement of the body, particularly the head. This situation makes the driving task unrealistic and unnatural.

5.1.2 Driving task

To verify that the reduction in driving workload with ACC could be evaluated from brain activity, we conducted an experiment that involved the use of a driving simulator simulating following a vehicle (Fig. 17).

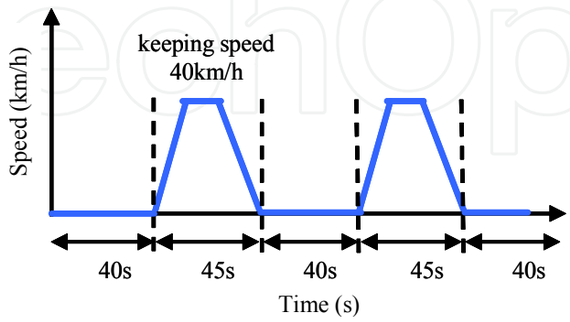

Fig. 17. Speed pattern of leading car

The main specifications of the driving simulator were as follows. Dimensions: 2,440 mm (W) × 2,280 mm (H) × 1,850 mm (D), front view: wide-field (138 degrees) screen projection, DLP projector with a total pixel count of 780,000 (XGA), rear view: 3 mirror independent LCD

display 640×480 pixel (VGA), computer graphics: redraw speed, 30-60 frames/s, simulation system: 6-axis motion base system using six electric screw cylinders.
Driving tests were conducted under two conditions: one involved following a vehicle while utilizing the ACC; and the other involved following a vehicle while driving without ACC. The subject performed practice runs to become somewhat skilful in handling the driving simulator and then drove twice under each condition. Brain activity during one condition was compared with that during the other condition.

5.1.3 Measurement method

Brain activity in the frontal lobe was measured using NIRS. Figure 18 depicts the scene of the experiment. The measuring instrument was the OMM-300 near-infrared imaging device (Shimadzu Corporation, Japan). Figure 19 illustrates the arrangement of optical-fiber units (3 × 9 matrix, 42 channels).
Numbers between the light-emitting fiber unit and the light-receiving fiber unit denote the measurement channels; measurements were performed through a total of 42 channels. Furthermore, driving performance was also recorded on the driving simulator while measuring brain activity. Four male subjects in their 20s participated; all were in healthy condition and had ordinary driving licenses.

Fig. 18. Experiment with driving simulator (driver follows the proceeding vehicle with and without ACC)

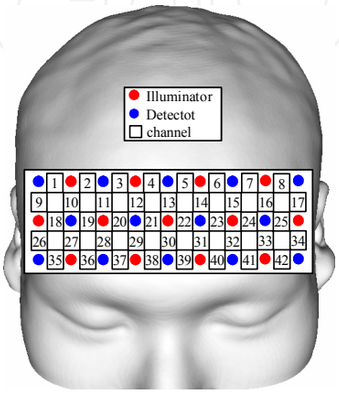

Fig. 19. Position of optical fibers and channels (driving task: 3×9 matrix, 42 channels)

5.1.4 Decomposition and reconstruction of NIRS signals

NIRS signals include signals that are unrelated to brain activity (e.g., noise of the measurement instrument, influences of breathing, and changes in blood pressure). These unrelated signals need to be removed to evaluate brain activity in detail. The measured NIRS signals were thus decomposed through MRA using discrete wavelet transform, and components related to the driving task were reconstructed. Group analysis using Z-score was then conducted for all subjects.

5.1.5 Results

Figure 20 presents the results of group analysis for four drivers without ACC, while Figure 21 presents the results with ACC. Figure 20(a) confirms that oxygenated hemoglobin increased when the subject drove without ACC and exhibited a high value in the latter half of the task. The brain function imaged in Figure 20(b) confirms that, as common brain activity, both outer portions of the frontal lobe became active during the driving task.

Figure 21(a) indicates that oxygenated hemoglobin did not increase while driving with the use of ACC. Also, the brain function image in Figure 21(b) reveals that the frontal lobe was less active than when the subject drove without ACC. This result may reflect the reduction of driving workload by ACC.

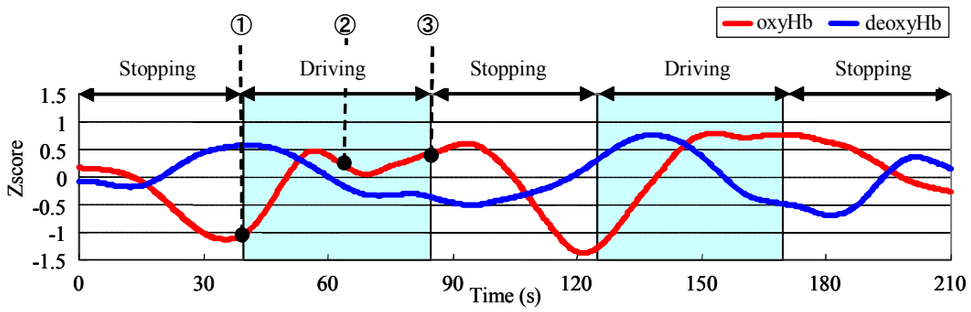

(a) Averaged reconstructed NIRS signal (channel 26)

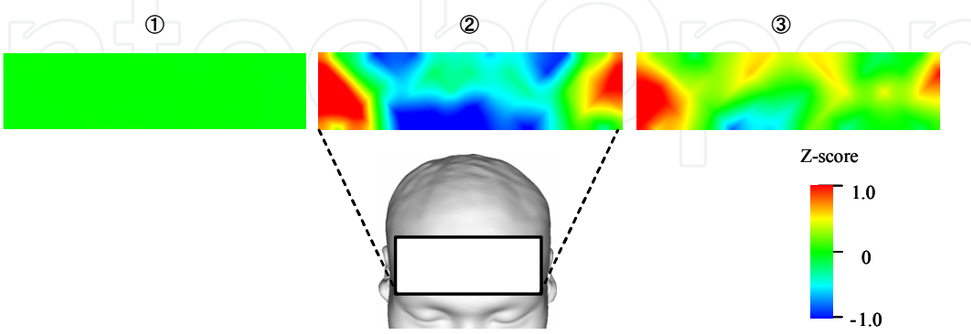

(b) Functional brain imaging

Fig. 20. Results of group analysis for four drivers without ACC system

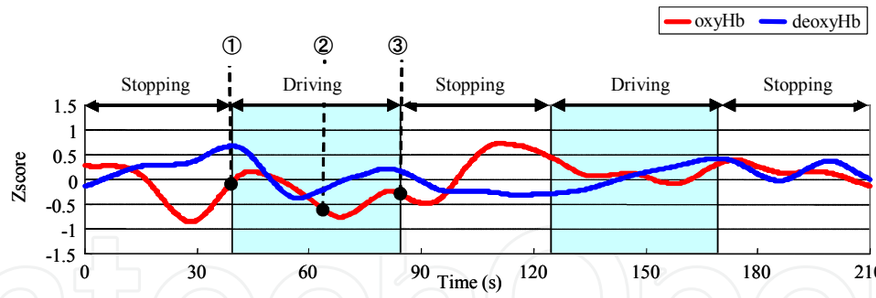

(a) Averaged reconstructed NIRS signal (Channel no. 26)

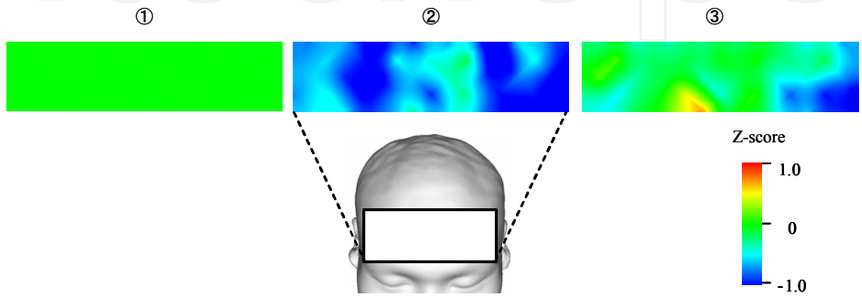

(b) Functional brain imaging

Fig. 21. Results of group analysis for four drivers with ACC system

5.2 Brain-Computer Interface (BCI) using NIRS

5.2.1 Background

Currently, the concept of BCIs is under intense study. BCIs extract activity from the human brain as cranial nerve information and use the information as inputs to control machinery and equipment. If this could enable the operation of machinery and equipment directly from cranial nerve information without the subject moving the hands and feet, such systems could be applied to care-taking robots for physically handicapped individuals.

BCI systems can be divided into two types. The invasive type reads cranial nerve information using electrodes embedded directly into the brain. The non-invasive type reads cranial nerve activity from the surface of the head using NIRS or electroencephalography (EEG). The invasive type offers high signal accuracy, but imposes heavy burdens on the user, such as the need for invasive procedures and the risk of infections after such procedures. The non-invasive form thus seems to have wider applicability.

In a study on the non-invasive type, Matsumura et al. extracted cranial nerve information using EEG and controlled a humanoid robot (Matsumura & Nakagawa, 2006). Many other studies of BCIs have used EEG. However, EEG may be greatly affected by movement of the user's body, and is vulnerable to electronic noise. In contrast, NIRS imposes fewer restrictions on body movement than EEG and is more resistant to electronic noise, so the load imposed on the user is less and electronic devices have no influence. The present study therefore focused on BCIs using NIRS.

In an earlier study, Nagaoka et al. developed an NIRS-BCI rehabilitation system (Nagaoka et al., 2010). In that study, electric stimuli corresponding to cranial nerve information were applied to the biceps brachii muscle of the user by setting a threshold on signals measured

from NIRS, in order to cause the elbow joint to move. Signals measured by NIRS are unstable, since signals components that are irrelevant to the subject (e.g., noise of measurement instruments, heartbeat, and respiration) are included. Moreover, no processing method for NIRS signals has yet been established. For these reasons, obtaining a highly accurate operation by merely setting a simple threshold on NIRS signals is difficult.

In this study, we assumed artificial arms for physically handicapped individuals and proposed a BCI system that would enable operation of the robot arms using NIRS to measure cranial nerve information in a non-invasive manner. Furthermore, we applied new signal-processing methods, such as multiresolution analysis with discrete wavelet transform and a brain activity-judging method that uses derivatives of NIRS signals, to achieve highly accurate on/off operations.

In imaging tasks where the subject performs imaging in the brain without moving the body, signal intensity is weak and the presence of brain activity is difficult to judge. We therefore first verified the effectiveness of the system and judging method in grasping tasks, which have high signal intensity, and then verified the identification accuracy of the system from tests that involve imaged grasping tasks, with consideration of applying the system.

5.2.2 A robot arm control using a NIRS-BCI system

Figure 22 depicts a robot arm control system that uses a NIRS-BCI system. This system is composed of a cerebral function measurement section, a feature extraction and recognition section, and a device control section. In the cerebral function measurement section, the oxygenated hemoglobin level of the user is measured using the OMM-3000 multichannel NIRS instrument made by Shimadzu Corporation, Japan. In the feature extraction and recognition section, the threshold is obtained by analyzing the original signal of oxygenated hemoglobin that was measured. When oxygenated hemoglobin after analysis exceeds the threshold obtained in the feature extraction and recognition section, the on signal is sent to the device control section to enable rotation of the joint of the robot arm (MR-999; Elekit, Japan).

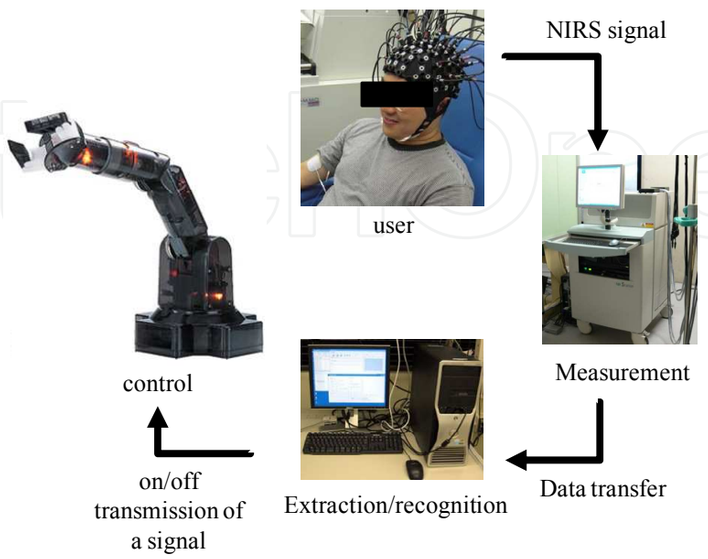

Fig. 22. Robot arm control using the NIRS-BCI system

Experiments were conducted using the robot arm control system depicted in Figure 22. Optical fibers were arranged in 4×4 matrices on the right and left sides to perform measurement, with a total of 48 channels.
Five trials were carried out, with each trial consisting of 10 s of pre-task rest, 30 s of task, and 10 s of post-task rest. The first two trials were defined as the learning stage, where the feature extraction and recognition section learned the fluctuation pattern of the user's oxygenated hemoglobin levels without moving the robot.
In the third and subsequent trials, the robot arm was rotated according to the learned pattern corresponding with oxygenated hemoglobin. Both grasping tasks and imaged grasping tasks were performed. The subject was instructed to rest during the rest time. The motor area was selected as the measurement site.

5.2.3 Judgment of brain activity

Judgment with a simple threshold

In the judgment method that used a simple threshold, the average oxygenated hemoglobin level in the first two trials and the standard deviation were converted to Z-scores, and the moving average was obtained. The threshold was set to 20% of the maximum oxygenated hemoglobin level during the first two trials; judgment was made in the third and subsequent trials, and an "on" state was judged when oxygenated hemoglobin level exceeded this threshold.
Changes in density of oxygenated hemoglobin level and the judgment results for imaged grasping tasks and actual grasping tasks are depicted in Figure 23. In Figure 23(a), "on" judgments were observed in the first and second trials, but not in the third trial. Next, in Figure 23(b), "on" judgments were made in all tasks from the first to third trials, but "on" and "off" judgments alternated within a short time, indicating instability. Furthermore, an "on" judgment was made during the rest period in the second trial, indicating erroneous judgments.

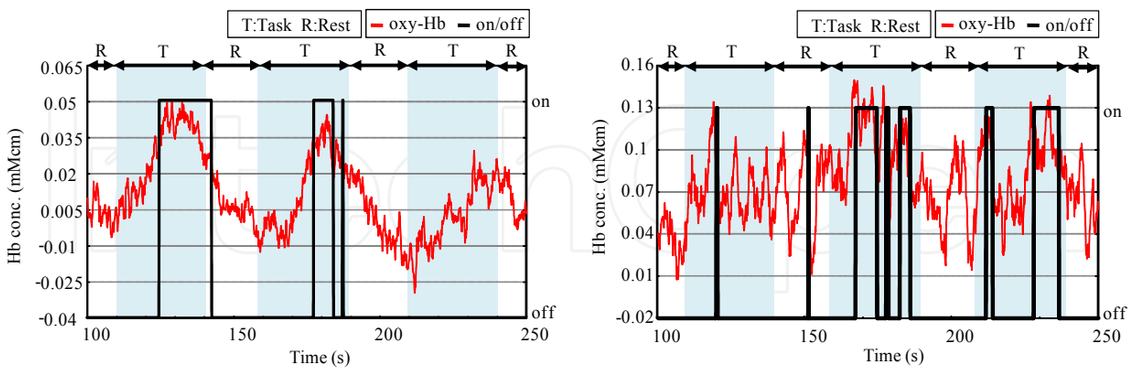

(a) Actual grasping tasks (b) Imagined grasping tasks

Fig. 23. Results for on/off decisions using a simple threshold

Judgment using oxygenated hemoglobin level and its derivative

NIRS can measure both change in density of oxygenated hemoglobin and that of deoxygenated hemoglobin; however, the change in density of oxygenated hemoglobin is highly correlated with the change in regional cerebral blood flow (rCBF) (Hoshi, 2001), and

an increase in rCBF reflects an increase in neural activity. We therefore focused on the oxygenated hemoglobin signal.

Furthermore, the derivative of oxygenated hemoglobin is highly correlated with the workload of the task as shown in Section 4.6, so we judged brain activity using two indices: oxygenated hemoglobin; and its derivative. First, NIRS signals include signal components that are irrelevant to brain activity (e.g., noise of measurement instruments, influences of respiration, and fluctuations of blood pressure). Signals were thus decomposed and reconstructed by MRA.

The original oxygenated hemoglobin signal and reconstructed oxygenated hemoglobin signal are depicted in Figure 24(a). In Figure 24(a), oxygenated hemoglobin includes not only brain activity, but also the effects of blood pressure, breathing and measurement noises. However, in Figure 24(b), the reconstructed oxygenated hemoglobin signal can be seen to be smoothed.

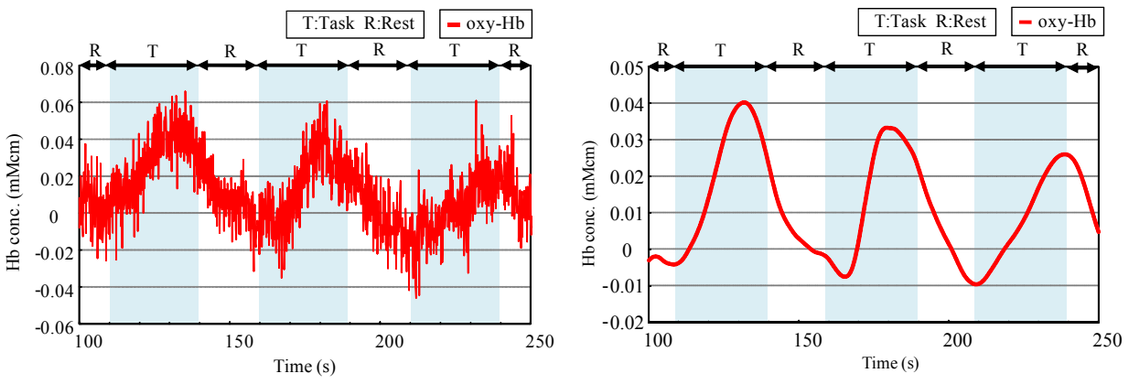

(a) Original oxy-Hb signal (b) Reconstructed oxy-Hb signal

Fig. 24. Changes in original and reconstructed oxygenated hemoglobin signals

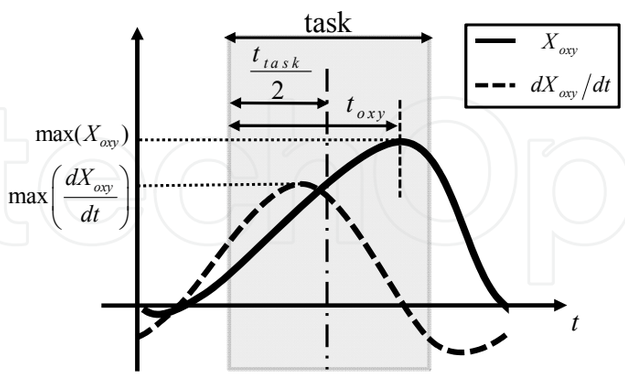

Fig. 25. Oxygenated hemoglobin concentration change due to neural activity

Changes in oxygenated hemoglobin and its derivative when the brain is activated are depicted in Figure 25. Oxygenated hemoglobin was defined as X_{oxy} and its derivative was defined as dX_{oxy}/dt. The threshold of oxygenated hemoglobin (denoted as y_1) and that of the derivative (denoted as y_2) were computed by $y_1 = K_1 \max(X_{oxy})$ and $y_2 = K_2 \max(dX_{oxy}/dt)$. K_1 and K_2 were weight factors that depended on the point where X_{oxy} reached a maximum.

The point where X_{oxy} reached a maximum was defined as $e = (t_{oxy} - t_{task}/2)/(t_{task}/2)$. Here, t_{task} was a time at which tasks were performed and t_{oxy} was a time from start of the task to when X_{oxy} reached a maximum. In this study, K_1 and K_2 were set to $K_1 = 0.8e + 0.2$ and $K_1 = -0.8e + 1$. If X_{oxy} reached maximum in the middle of the task, y_1 was 20% of the maximum value of X_{oxy}. If X_{oxy} reached maximum at the end of the task, y_2 was 20% of the maximum value of dX_{oxy}/dt. The on/off decision (on = 1, off = 0) was made by Y (= 1: $X_{oxy}>y_1$ or $dX_{oxy}/dt>y_2$, = 0: otherwise).

The judgment result for grasping tasks when the proposed judgment method was applied is depicted in Figure 26(a), and that for imaged grasping tasks is depicted in Figure 26(b).

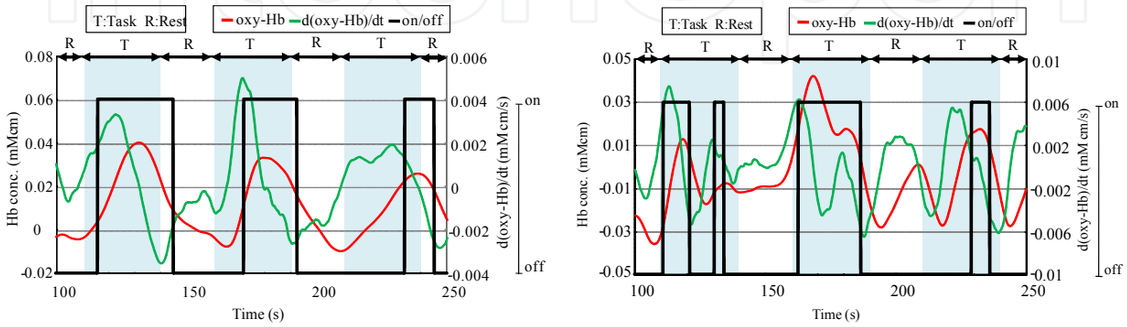

(a) Actual grasping tasks (b) Imagined grasping tasks

Fig. 26. Result of on/off decision using oxygenated hemoglobin and its derivative

In contrast to the judgment method where a simple threshold was imposed on oxygenated hemoglobin in grasping tasks (Fig. 23(a)), "on" judgments were confirmed during the first and all subsequent tasks with the method depicted in Figure 26(a). However, "on" judgments were made continually for 5 s after completion of the task in each trial, indicating that erroneous judgments may be made. The judgment method thus needs further refinement.

In contrast to the judgment method where a simple threshold was imposed on oxygenated hemoglobin in imaged grasping tasks (Fig. 23(b)), more stable judgment was made in Figure 26(b), and the problem of alternating "on" and "off" judgments within a short time was reduced.

6. Conclusions

A signal-processing method to extract task-related components with MRA based on discrete wavelet transform is proposed for NIRS. Integration of data from multiple subjects using Z-scores was then developed for statistical group analysis.

Brain activity of subjects with workloads comprising different levels of mental calculation tasks were measured using NIRS and fMRI. NIRS images constructed using the proposed method agreed with fMRI images at different workload levels. Those results show that the proposed method is effective for evaluating brain activity measured by NIRS.

Comparison between NIRS signal (cerebral blood flow) and skin blood flow showed that skin blood flow does not affect NIRS signal in the recognition task.

Changes in brain activity in connection with workload were compared with the subjective evaluation of workload by NASA-TLX. Good correlation was observed between brain

activity detected by NIRS and workload scores obtained from NASA-TLX. This result indicates the possibility of evaluating workload from cerebral blood flow signals obtained using NIRS.

Whether the reduction of driving workload by ACC can be evaluated from brain activity was evaluated through experiments using a driving simulator. The results revealed that while the outer portions of the frontal lobe were active in connection with driving performance when the subject drove without ACC, no activity related to driving performance was seen with the use of ACC. These results suggest the possibility of evaluating driving-assistance systems through the evaluation of driving workload from measurement of brain activity using NIRS.

We developed MRA using discrete wavelet transform as a real-time post-signal processing for NIRS-BCI system and applied this approach to control of a robot arm. With a judgment method that used a simple threshold, no stable operation could be obtained for grasping tasks or imaged grasping tasks.

We proposed a judgment method that uses two indices (oxygenated hemoglobin and the derivative of oxygenated hemoglobin) for judging brain activity, and adjusts the threshold of oxygenated hemoglobin and its derivative depending on the point of maximum oxygenated hemoglobin during the task. Results indicate that our proposed method enables more accurate judgments than use of a simple threshold. We thus confirmed the feasibility of our proposed method for a NIRS-BCI system.

7. Acknowledgment

This work was supported by the Nihon University Multidisciplinary Research Grant in 2006, 2007 and 2010.

8. References

Hoshi, Y., Kobayashi, N., Tamura, M. (2001). Interpretation of nearinfrared spectroscopy signals, A study with a newly developed perfused rat brain model, *Journal of Applied Physiology*, Vol.90, No.5, pp.1657-1662

Tamura, M. (2003). Functional near-infrared spectoroscopy, *Advances in Neurological Sciences,* Series C, Vol.47, No.6, pp.891-901

Kojima, T., Tsunashima, H., Shiozawa, T., Takada, H. and Sakai, T. (2005). Measurement of Train Driver's Brain Activity by Functional Near-Infrared Spectroscopy (fNIRS), *Optical and Quantum Electronics*, Vol.37, No.13-15, pp. 1319-1338

Kojima, T., Tsunashima, H., Shiozawa, T. (2006). Measurement of train driver's brain activity by functional near-infrared spectroscopy (fNIRS), *COMPUTERS IN RAILWAYS X*, WIT Press

Shimizu, T., Hirose, S., Obara, H., Yanagisawa, K., Tsunashima, H., Marumo, Y., Haji. T. and Taira, M. (2009). Measurement of Frontal Cortex Brain Activity Attribute to the Driving Workload and Increased Attention, *SAE paper* NO. 2009-01-054

Takahashi, K., Watanabe, N. and Harada, T. (2006). Preliminary experiment of the evaluation of a VR based training system using brain activity, *Virtual Reality Society of Japan Annual Conference*, Vol. 11 pp. 354-355, ISSN 1349-5062, Japan, 2006

Mallat, S. (1998). *A Wavelet Tour of Signal Processing,* Academic Press, ISBN 978-0124666061, USA

Mallat, S. (1989). A theory for multiresolution signal decomposition: the wavelet representation, *IEEE Transactions on Pattern Recognition and Machine Intelligence*, Vol.11, No.7, pp.674-693

Jöbsis, FF. (1977). Non-invasive infrared monitoring of cerebral and myocardial oxygen sufficiency and circulatory parameters, *Science*, Vol.198, pp.1264-1267

Kohno, S. , Ishikawa, A., Tsuneishi, S., Amita, T., Shimizu, K. and Mukuta, Y. (2006). Application development of functional near-infrared imaging system, *Shimadzu Review*, Vol. 63, No.3.4, pp.195-200

Huettel, S. A. (2004). *Functional Magnetic Resonance Imaging,* Sinauer Associate, Inc., ISBN 978-0878932887, USA

Daubechies, I. (1992). *Ten Lectures on Wavelets,* CBMS-NSF Regional Conference Series In Applied Mathematics; Society for Industrial and Applied Mathematics, No.61, ISBN 978-0898712742

Mallat, S. (1989). A theory for multiresolution signal decomposition: the wavelet representation, *IEEE Transactions on Pattern Recognition and Machine Intelligence*, Vol.11, No.7, pp.674-693

Uchiyama, Y., Ebe, K., Kozato, A., Okada, T., Sadato, N. (2003). The neural substrates of driving at a safe distance: a functional MRI study, *Neuroscience Letters*, Vol.352-3, pp.199-202

Spiers, H. J. and Maguire, E. A. (2007). Neural substrates of driving behaviour, *Neuro Image*, No.36, pp.245-255

Matsumura, H. and Nakagawa, M. (2006). An EEG-based Humanoid Robot Control System, *The institute of electronics, information and communication engineers*, Vol.106, No.345, pp.63-68, ISSN 09135685

Nagaoka, T., Sakatani, K., Awano, T., Yokose, N., Hoshino, T., Murata, Y., Katayama, Y., Ishikawa, A., Eda, H. (2010). Development of a new rehabilitation system based on a brain-computer interface using near infrared spectroscopy, *Advances in Experimental Medicine and Biology*, Vol.662, pp. 497-503

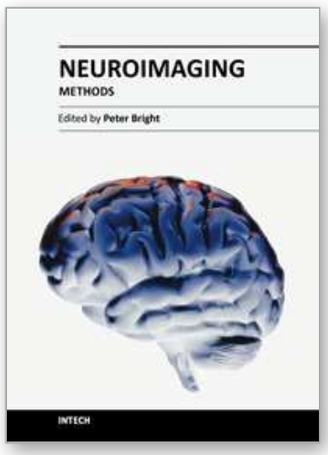

Neuroimaging - Methods
Edited by Prof. Peter Bright

ISBN 978-953-51-0097-3
Hard cover, 358 pages
Publisher InTech
Published online 17, February, 2012
Published in print edition February, 2012

Neuroimaging methodologies continue to develop at a remarkable rate, providing ever more sophisticated techniques for investigating brain structure and function. The scope of this book is not to provide a comprehensive overview of methods and applications but to provide a 'snapshot' of current approaches using well established and newly emerging techniques. Taken together, these chapters provide a broad sense of how the limits of what is achievable with neuroimaging methods are being stretched.

How to reference
In order to correctly reference this scholarly work, feel free to copy and paste the following:

Hitoshi Tsunashima, Kazuki Yanagisawa and Masako Iwadate (2012). Measurement of Brain Function Using Near-Infrared Spectroscopy (NIRS), Neuroimaging - Methods, Prof. Peter Bright (Ed.), ISBN: 978-953-51-0097-3, InTech, Available from: http://www.intechopen.com/books/neuroimaging-methods/measurement-of-brain-function-using-near-infrared-spectroscopy-nirs-

INTECH
open science | open minds

InTech Europe
University Campus STeP Ri
Slavka Krautzeka 83/A
51000 Rijeka, Croatia
Phone: +385 (51) 770 447
Fax: +385 (51) 686 166
www.intechopen.com

InTech China
Unit 405, Office Block, Hotel Equatorial Shanghai
No.65, Yan An Road (West), Shanghai, 200040, China
中国上海市延安西路65号上海国际贵都大饭店办公楼405单元
Phone: +86-21-62489820
Fax: +86-21-62489821

IntechOpen